Whole genome sequencing uncovers the structural and transcriptomic landscape of hexaploid wheat/*Am. muticum* introgression lines

Benedict Coombes[1], John Fellers[2], Surbhi Grewal[3], Rachel Rusholme-Pilcher[1], Stella Hubbart-Edwards[3], Cai-yun Yang[3], Ryan Joynson[1], Ian P. King[3], Julie King[3], Anthony Hall[1*]

[1]Earlham Institute, Norwich, Norfolk, NR4 7UZ, UK

[2]USDA–ARS Hard Winter Wheat Genetics Research Unit, Manhattan, KS 66506, USA

[3]School of Biosciences, The University of Nottingham, Sutton Bonington Campus, Loughborough, Leicestershire, LE12 5RD, UK

*Corresponding author – anthony.hall@earlham.ac.uk

Abstract

Wheat is a globally vital crop, but its limited genetic variation creates a challenge for breeders aiming to maintain or accelerate agricultural improvements over time. Introducing novel genes and alleles from wheat's wild relatives into the wheat breeding pool via introgression lines is an important component of overcoming this low variation but is limited by poor genomic resolution and limited understanding of the genomic impact of introgression breeding. By sequencing 17 hexaploid wheat/*Ambylopyrum muticum* introgression lines and the parent lines, we have precisely pinpointed the borders of introgressed segments. We report a genome assembly and annotation of *Am. muticum* that has facilitated the identification of *Am. muticum* resistance genes commonly introgressed in lines resistant to stripe rust. Our analysis has identified an abundance of structural disruption and homoeologous pairing across the introgression lines, likely caused by the suppressed Ph1 locus. mRNAseq analysis of six of these introgression lines revealed that introgressed genes tend to be downregulated, shifting the expression balance of triads towards suppression of the introgressed region, with no discernible compensation in the expression of the homoeologous copies. This analysis explores the genomic impact of introgression breeding and provides an affordable way for breeders to better characterise introgression lines and more effectively deploy wild relative variation.

Introduction

Triticum aestivum L. (bread wheat) is a vital crop, providing around 20% of calories and 25% of protein consumed globally (*1*). Improvements to wheat since the late 19th century have largely come from conventional breeding strategies, but these improvements rely on ample genetic variation in the primary gene pool (*2*). The hexaploid bread wheat grown today derives from just one or two polyploidisation events ~10,000 years ago between the tetraploid *Triticum turgidum* and the diploid *Aegilops tauschii* (*3*). The limited diversity stemming from this genetic bottleneck has been compounded over time by intensive breeding. Pressure on

breeders to prioritise advanced breeding material (*4*) for more rapid development of elite uniform, high quality varieties that perform competitively has limited the introduction of genetic variation from external sources. The genetic variation that does exist in modern wheat material is rapidly being exhausted, evident in plateauing yield improvements that left unchecked, will be insufficient to meet global demands (*5*). Wild relative introgression breeding will be a major component of overcoming this genetic constraint in the years to come, enabling breeders to access the secondary and tertiary gene pools of wheat (*2*, *4*) and incorporate novel alleles or genes into modern breeding material.

There are many examples of the successful transfer of wild relative genes into wheat since first pioneered by E.R. Sears (*6*–*10*). However, challenges associated with the high-throughput production and verification of introgression lines, in addition to the linkage drag of introgressed segments, has limited the widespread adoption of introgression breeding. Utilising recombination mutants and high-throughput marker methods, introgressing entire wild relative genomes into wheat as stably inherited, homozygous segments is now possible (*11*, *12*). These sets of lines provide the raw material required for the incorporation of alien variation into breeding programmes. Segments in these lines that confer phenotypes of interest can be identified. Lines with overlapping segments can then be crossed to break down large segments (*13*), resulting in genes of interest captured in short introgressed segments with reduced linkage drag, ready to be crossed into elite lines and deployed in breeding programmes.

Identifying the introgressed content of each introgression line is important for the effective utilisation of these lines. Insufficient marker density and low resolution of genomic *in situ* hybridisation (GISH) limits the resolution at which segments can be identified. Genotyping, using methods such as Kompetitive allele specific PCR (KASP), is a cheap and effective way to screen lines for introgressed segments. Determining the precise size and positions of segments and refining positions of overlap between introgression lines is important when relating to phenotypic data to narrow down regions containing genes of interest. Identifying introgression boundaries at a higher resolution will allow lines with overlapping segments to be identified; these can be crossed to break down segments and capture genes of interest in smaller segments with reduced linkage drag.

Wild relative genes have undergone selection in a different environment to the agricultural setting in which elite wheat lines are selected and thus may be deleterious, or be, at the very least imperfect replacements of their wheat orthologue when deployed in field conditions. Therefore, many genes introgressed along with a gene of interest will contribute to reduced agronomic performance of a line. This reduced performance will be driven by differences both in the encoded protein and in the pattern of expression of the introgressed gene compared to the wheat orthologue it replaced. In addition to these cis effects of introgression, disruptions to established regulatory networks and resulting trans effects on the expression of background wheat genes will likely contribute to altered performance.

Ordinarily, hexaploid wheat behaves as a diploid during meiosis. The *Pairing Homoeologous 1* (*Ph1*) locus is largely responsible for this behaviour, restricting synapsis and crossovers to homologous chromosomes (*14*). A

67 suppressed or deleted *Ph1* locus enables recombination between wheat chromosomes and non-homologous
68 wild relative chromosomes and has been a major tool used for decades to transfer wild relative genes into
69 wheat (*15*). However, this also enables homoeologous chromosomes to pair and recombine leading to
70 transmission of chromatin between the subgenomes of wheat (*16*) and deletions/duplications where synteny
71 between homoeologous chromosomes breaks.

72 Here, we have conducted a high-resolution genomic analysis on 17 *Am muticum*/hexaploid wheat
73 introgression lines (*11*, *12*), utilising whole-genome sequencing (WGS) data from the introgression lines and
74 the parent lines and a draft genome assembly of *Amblyopyrum muticum* [(Boiss.) Eig.; *Aegilops mutica* Boiss;
75 2n=2X=14; genome TT], a wild relative of wheat belonging to its tertiary gene pool. Phenotypic screening of
76 *Am. muticum* introgression lines (*17*) has revealed resistances to leaf, stem and stripe rust not observed in the
77 parental wheat lines and thus likely conferred by introgressed genes. KASP genotyping to identify segments
78 has been conducted on many of these lines (*18*). Through this analysis, we have pinpointed introgression
79 segment junctions to a higher resolution than previously possible, in many cases within a single pair of reads,
80 demonstrating segments of variable size that overlap between introgression lines, which explains some
81 differences in resistance phenotype seen between lines. These overlaps will enable these segments to be
82 further broken down by crossing introgression lines together. Using *in silico* karyotyping, we have shown that
83 large-scale structural disruption is ubiquitous across the lines, including deletions and duplications up to
84 whole-chromosome size and homoeologous recombination likely facilitated by the suppressed *Ph1* locus. A
85 genome assembly and gene annotation of *Am. muticum* has enabled us to identify introgressed resistance
86 genes in stripe, stem and leaf rust resistant lines that may represent novel resistance conferred by *Am.*
87 *muticum* genes. Analysis of gene expression of six introgression lines compared to the wheat parent lines has
88 revealed a tendency for introgressed genes to be downregulated or silenced compared to the wheat
89 orthologue they replace, with minimal balancing of the homoeologous copies in the remaining subgenomes.

90 Results

91 Whole genome sequencing facilitates high resolution introgression detection

92 To reveal *Am. muticum* segments within introgression lines using WGS data, we developed a workflow that
93 utilises mapping coverage and single nucleotide polymorphism (SNP) information from the introgression line
94 and the wheat parents. If a wheat segment is replaced by an *Am. muticum* segment the mapping coverage will
95 drop in that region due to structural variation and breaks in synteny between wheat and *Am. muticum*. Due to
96 the homozygous nature of the lines, homozygous muticum-specific SNPs are indicative of the site of
97 introgression. Reads derived from an introgressed segment that aberrantly map to a non-introgressed region
98 will map at the same position as the wheat reads coming from that region and result in heterozygous SNP calls
99 with muticum-specific and wheat-specific alleles found at the same position. Therefore, to locate
100 introgressions, we searched for genomic blocks with reduced mapping coverage, homozygous *Am. muticum*-
101 specific SNPs and few heterozygous *Am. muticum*-specific SNPs. We identified introgressions using 1Mbp

genomic windows and then defined the borders to a higher resolution using 100Kbp genomic windows. Figure 1A shows an example of this macro-level visualisation of introgression line DH65, which has a 51.29Mbp segment on the telomere of the short arm of chr4D, and a 139.6Mbp monosomic deletion on the short arm of chr5B. Macro-level genome plots for all lines can be seen in fig. S1.

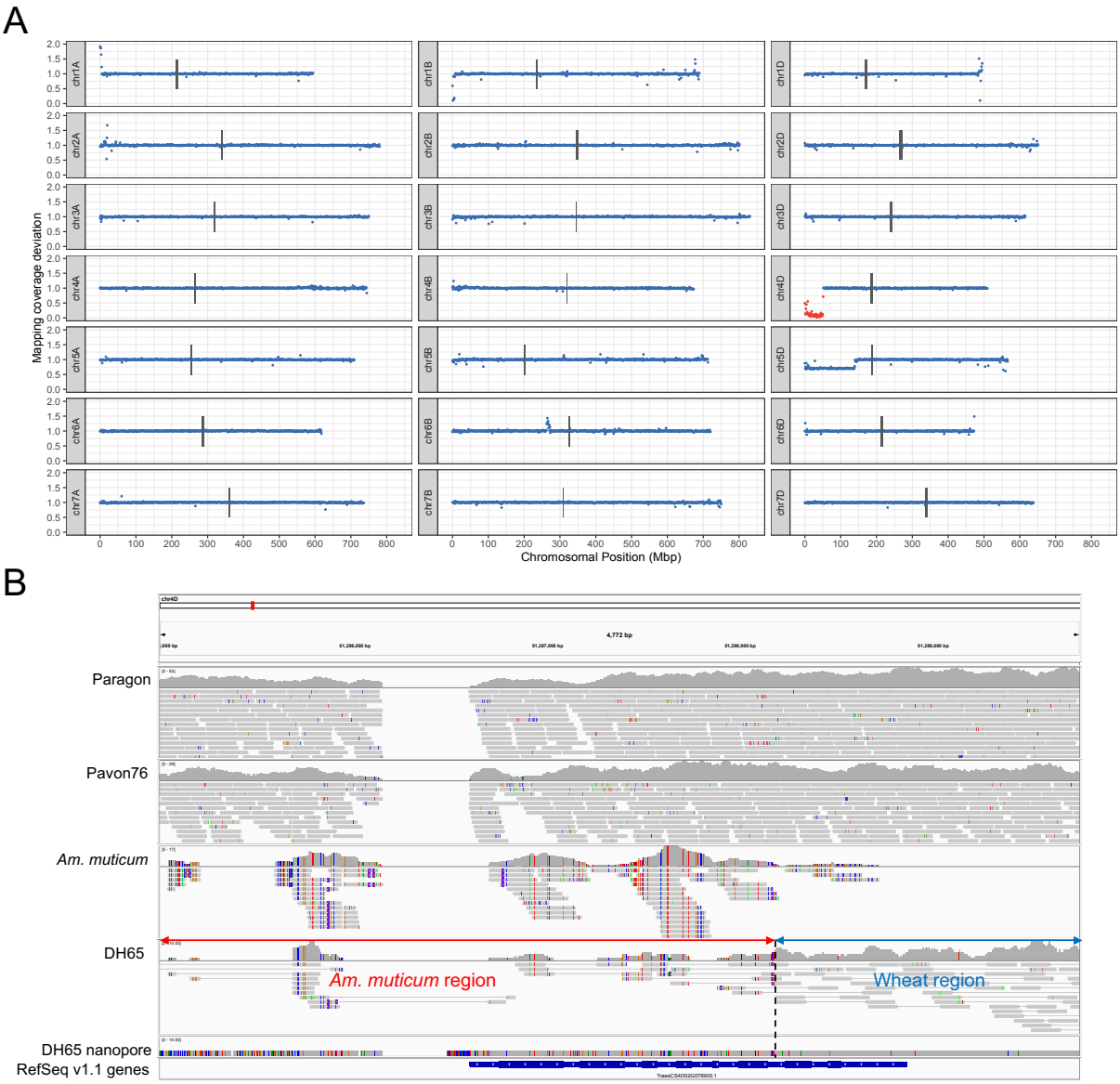

107 **Fig. 1. Identifying introgressed *Am. muticum* segments using whole-genome sequencing data. A** Visualising introgressed segments and structural variation in introgression lines using WGS sequencing data. Each point represents the deviation in mapping coverage compared to the parent lines in 1Mbp windows across Chinese Spring RefSeq v1.0. Windows within assigned *Am. muticum* introgression blocks are coloured red. Introgression line DH65, which has a 51.29Mbp introgressed segment on chr4D and a 139.6Mbp monosomic on chr5D. **B** IGV image showing junction at the right-hand side of chr4D segment in the introgression line DH65 (fig. 1A), spanned by both illumina and nanopore data from DH65. The first four tracks show mapped illumina WGS data, the fifth track shows assembled nanopore contig for DH65 and the bottom track shows high confidence genes from the RefSeq v1.1 annotation.

108 Using this approach, we confirm the existence of 100% of segments previously identified with KASP genotyping
109 (*18*). However, we were able to resolve the locations of segment junctions to a much higher resolution than
110 previous methods, due to the limited marker density available for KASP genotyping and the inability of GISH to
111 resolve segments below ~20Mbp. In addition, we were able to uncover two previously unreported segments
112 that have been subsequently validated by KASP genotyping (*18*); a 17.39Mbp on the telomere of chr7D of
113 DH195 and a 22.68Mbp segment on the telomere of chr5D in DH121. We also identified a new 3.99Mbp
114 segment on chr6D of DH15 that we subsequently validated using 2 KASP markers, WRC1873 and WRC1890. All
115 precise segment positions are listed in table S2.

116 By manually searching the boundary regions using IGV, we were able to identify segment end positions for
117 33/42 segment ends (78.6%). Looking solely at crossovers (excluding telomere substitutions) and excluding
118 junctions from non-independently derived segments, we could identify the precise crossover point between
119 wheat and *Am. muticum* in 12/17 (70.6%) cases. Of the remaining junctions, two were narrowed down to
120 within 100kbp and three had complex structures with duplication events that prohibited precise localisation.
121 Out of the 12 high resolution junctions, 11 (91.7%) were within 670bp upstream or downstream of a wheat
122 gene, with 8 falling within the gene body itself, suggesting that crossover points may be localised to genes. The
123 remaining junction was 6.75Kbp downstream from the nearest gene.

124 For line DH65, the pinpointed junction was validated with nanopore data (fig. 1B). 7x coverage of nanopore
125 sequencing data for DH65 was produced and mapped to the RefSeq v1.0 along with the illumina data.
126 Nanopore reads spanned the breakpoint between *Am. muticum* and wheat at the right-hand side of the
127 51.6Mbp chr4D segment, adding confidence to the illumina identification. We assembled these mapped
128 nanopore reads using wtdbg2 (*19*) with relaxed parameters to include reads that were clipped due to high
129 divergence between wheat and *Am. muticum*, producing a contig that spans the junction. The nanopore contig
130 spans the entire junction, including regions to which neither the illumina reads from *Am. muticum* or DH65
131 map. These regions appear to have elevated SNP density, explaining the gaps in mapping.

132 For introgression lines with KASP genotyping verification, WGS data may offer an affordable tool to aid
133 breeders to identify precise location and size of these segments. To assess the sequencing depth requirements
134 and locate the position and size of introgressed segments using coverage deviation alone, we downsampled
135 the paired-end Illumina sequencing data from 2 lines for which we have identified very precise positions of the
136 junction borders; DH65, and DH92, to 1x, 0.1x, 0.01x and 0.001x to choose the lowest depth at which we could
137 still resolve segment position. 0.01x was the lowest depth that still provided good resolution (fig. S2).

138 Introgression crossing induces large chromosomal aberrations and homoeologous
139 pairing/recombination

140 In addition to introgression sites, we have identified large deletions and duplications, many of which were
141 whole arm or whole chromosome in scale, based on the deviations in mapping coverage not attributable to

142 introgressions. Within the 17 lines examined, 12 lines (70.6%) have 1 or more very large chromosomal
143 aberrations exceeding 140Mbp. These include 3 examples of whole chromosomes being duplicated, along with
144 the corresponding deletion of one of its homoeologous chromosomes (fig. 2A), 2 arm or near-arm deletions
145 (fig. 2B), 2 near arm monosomies at identical positions between 2 independently derived lines (fig. 2C), and 2
146 whole-chromosome monosomies (fig. 2E).

147

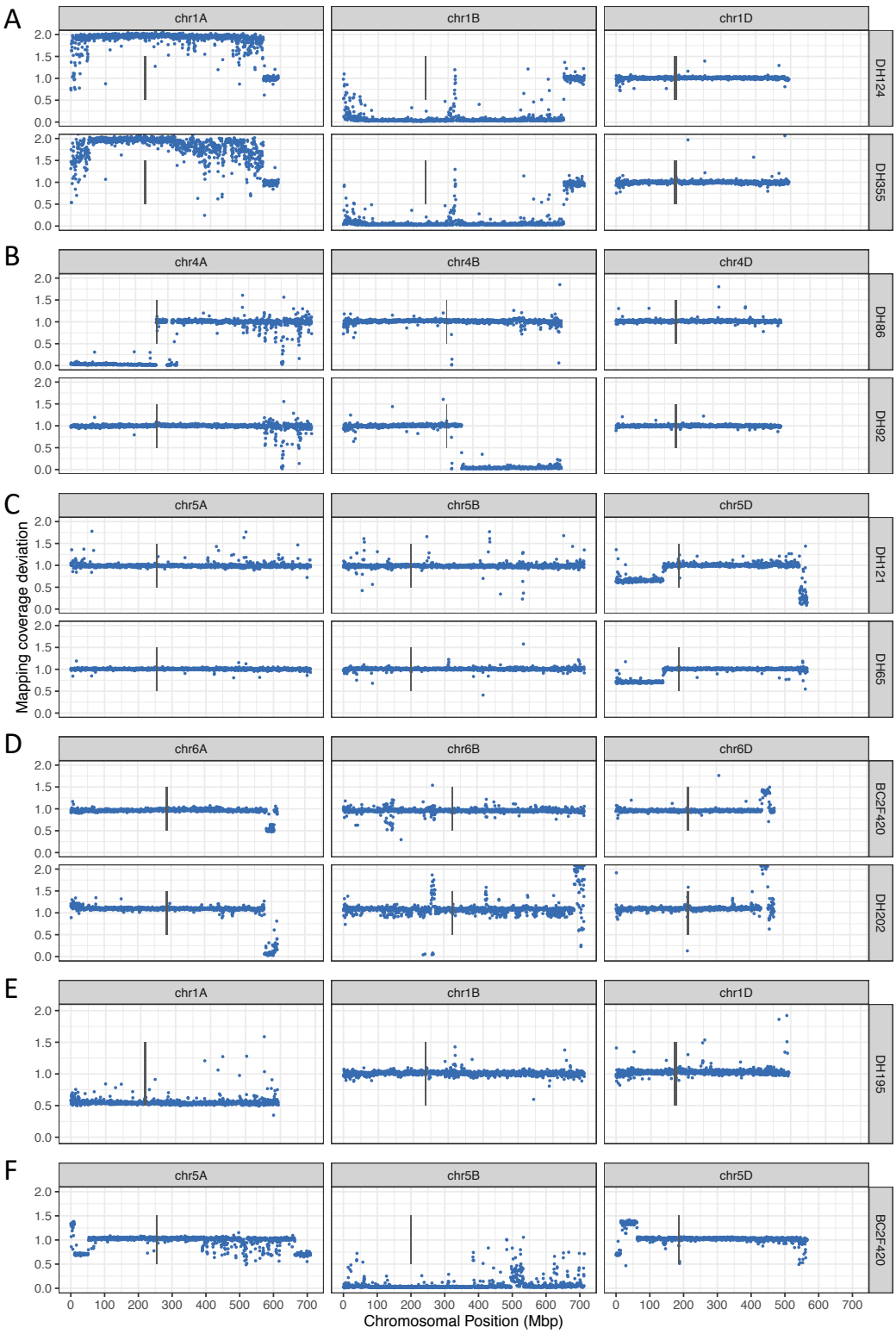

Fig. 2. Large chromosomal aberrations induced by introgression crossing. Each point shows mapping coverage deviation compared to the wheat parents in 500Kbp windows across the genome. **A** Corresponding duplication and deletion seen in both DH lines of BC3 pair, caused by pairing of a duplicated chr1A and chr1B. Mapping coverage deviation of 1 at the end of chr1A and chr1B indicates a large translocation between chr1A and chr1B has taken place in duplicated chr1A+chr1B pair and discontiguous mapping coverage deviation change towards beginning of chr1A and chr1B suggests lots of smaller translocation events. **B** Arm deletions on homoeologous chromosomes of DH pair. Possibly caused by pairing of chr4A and chr4B due to inverted synteny between these chromosomes. **C** Monosomic deletions at the same position in two independently derived lines. **D** Signal of duplicated translocations within homoeologous group 6, at similar positions in two independently derived lines. **E** Monosomic deletion of chr1A in DH195. **F** Complex chromosome structure, with a chimeric chr5A-chr5D replacing chr5B.

148

149 Homoeologous translocations resulting in the non-reciprocal transfer of genetic material can be detected
150 through mapping coverage deviation, indicated by a duplication and deletion in corresponding homoeologous
151 regions. We can also use differences within a DH pair (table S1) to infer what genetic events must have taken
152 place to give rise to the segregation patterns we see from DH lines derived from the same BC3 line. We see
153 evidence of homoeologous pairing both from duplicated/deleted pairs of chromosomes, such as in DH355 and
154 DH124 (fig. 2A) and from signatures of duplicated translocations, such as in DH202 and BC2F420 (fig. 2D). In
155 BC2F420, the event involves two chromosomes, and in DH202 it involves all three chromosomes in the
156 homoeologous group, where a region on chr6B and chr6D have duplicated and translocated side by side
157 replacing the homoeologous regions on chr6A.

158 ## Genome assembly and annotation of Am. muticum:

159 To facilitate identification of introgressed genes both for differential expression analysis and to find candidate
160 introgressed resistance genes, we produced a draft genome assembly for *Am. muticum* comprising most of the
161 gene space. 178Gbp of Oxford Nanopore reads were produced for *Am. muticum* accession JIC 2130012
162 (previously *Aegilops mutica;* GRU Store Code: T2130012). 156Gbp of these reads passed filtering and were
163 assembled using Flye (*20*). After polishing the resulting assembly with long and short reads and resolving
164 haplotigs, the assembly comprised 96,256 contigs and was 2.53Gbp in length, with an N50 of 75.5Kbp.
165 Mapping the nanopore reads back to the assembly and computing coverage across single-copy genes allowed
166 us to estimate the genome size at ~4.99Gbp. This is smaller than the c-value estimate for *Ae. mutica* of
167 6.174Gbp (*21*), suggesting variation in genome size between accessions. This is supported by variation in c-
168 value seen across wild *Aegilops tauschii* accessions (*21*). Although heavily collapsed, spanning just 50.1% of the
169 estimated genome size, BUSCO analysis (*22*) revealed that 94.2% of the expected gene space was assembled
170 unfragmented. Gene annotation using root and shoot transcripts, proteome, and ab initio evidence resulted in
171 63,032 gene models, 48,606 of which received transferred functional annotations from other well annotated
172 species. 26,597 *Am. muticum* genes were identified as orthologous to a corresponding wheat gene and
173 assigned to an orthologue pair.

174 ## Expression of introgressed genes and trans-regulatory impact on the transcriptome

175 To explore how introgressed genes are expressed and to understand the impact of introgression crossing on
176 the wheat transcriptome, we produced mRNAseq data for six of the introgression lines. *Am. muticum* genes
177 introgressed into each line were identified using orthologue assignments and DNA read mapping evidence.
178 RNA was mapped to a pseudo genome (ABDT) constructed by concatenating RefSeq v1.0 with the draft *Am.*
179 *muticum* genome assembly; this allows us to distinguish RNA deriving from wheat from RNA deriving from *Am.*
180 *muticum* genes. Differential expression was called between each introgression line and the wheat parent lines
181 using DESeq2 (*23*), substituting expression counts of wheat genes in introgressed regions with those of the
182 introgressed *Am. muticum* orthologue. Between 20.1% and 32.9% (27.2% across all lines) of introgressed
183 genes were called as differentially expressed (abs($\log_2$FC) >= 1 and adj. p-value <= 0.05 in both parental

comparisons) when compared to the expression in the parent lines of the wheat orthologue they replaced (fig. 3). Between 57.1% and 87.3% (73.5% across the lines) of these differentially expressed introgressed genes were downregulated or silenced in the introgression line.

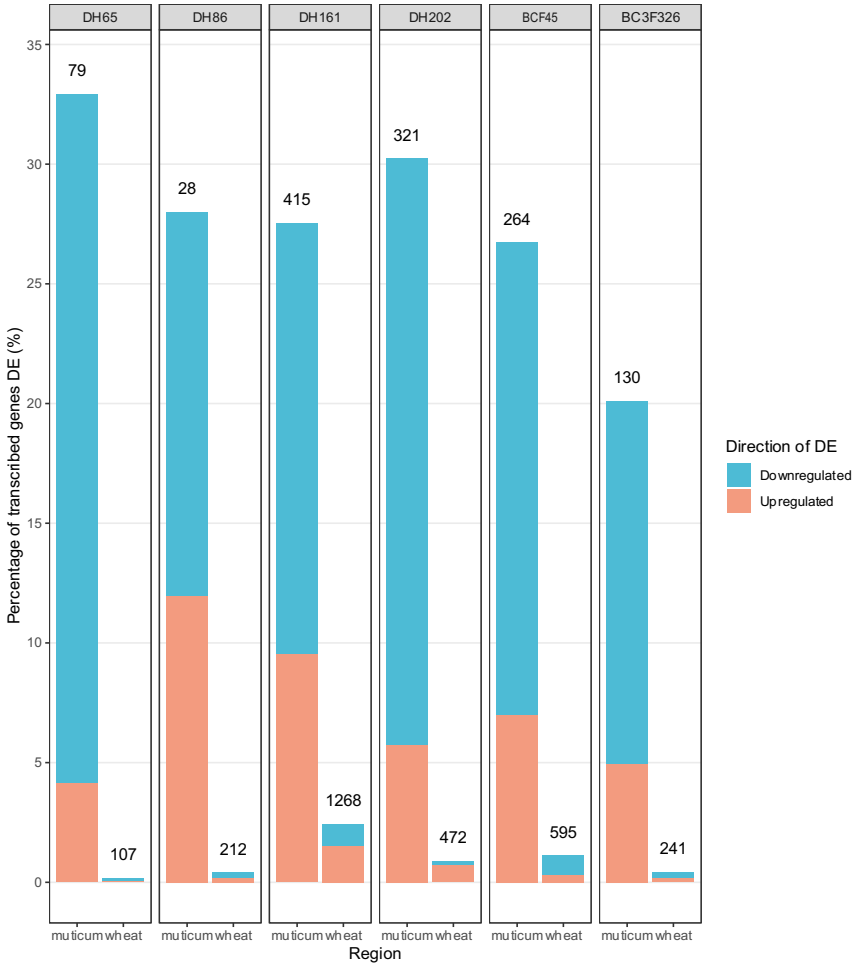

Fig. 3. Differential expression within introgression lines. Differential expression in 6 introgression lines, looking at introgressed genes compared to the orthologue they replaced in the parent lines, and background wheat genes compared to the expression in the wheat parent lines. The height of the bar represented the percentage of genes differentially expressed within introgressed and background regions for each line. The number above each bar is the number of genes called as differentially expressed.

188 We hypothesised that suppression of wheat genes in an introgressed or deleted region would lead to a change
189 in the expression of homoeologous copies of that gene in the other subgenomes to compensate for the loss of
190 expression and partially or completely restore the overall level of expression across the triad. The results of
191 multiple approaches support a lack of overall rebalancing of the triad following suppression of one of the
192 copies, both in the 400Mbp introgressed region on chr5D of BC3F45 and in the deletion of chr7D in DH161 (fig.
193 4). In the introgression, there were 262 triads with the D copy introgressed and called as downregulated; just 1
194 (0.382%) of these triads had one or more homoeologues called as upregulated; this compares to 4 (0.0509%)
195 triads out of 7863 background triads having the A or B homoeologue upregulated. For the deletion, out of
196 1294 triads with D copy deleted and therefore not expressed, just 5 triads had one or more homoeologues
197 upregulated (0.386%); this compares to 13 triads (0.170%) out of 7637 background triads having the A or B
198 homoeologue upregulated. Despite the percentage of upregulated homoeologues being lower in the
199 background, the difference is not significant (Fisher's exact test two-tailed p-values of 0.151 and 0.167,
200 respectively) and the number of triads with upregulated homoeologues is very small regardless.

201

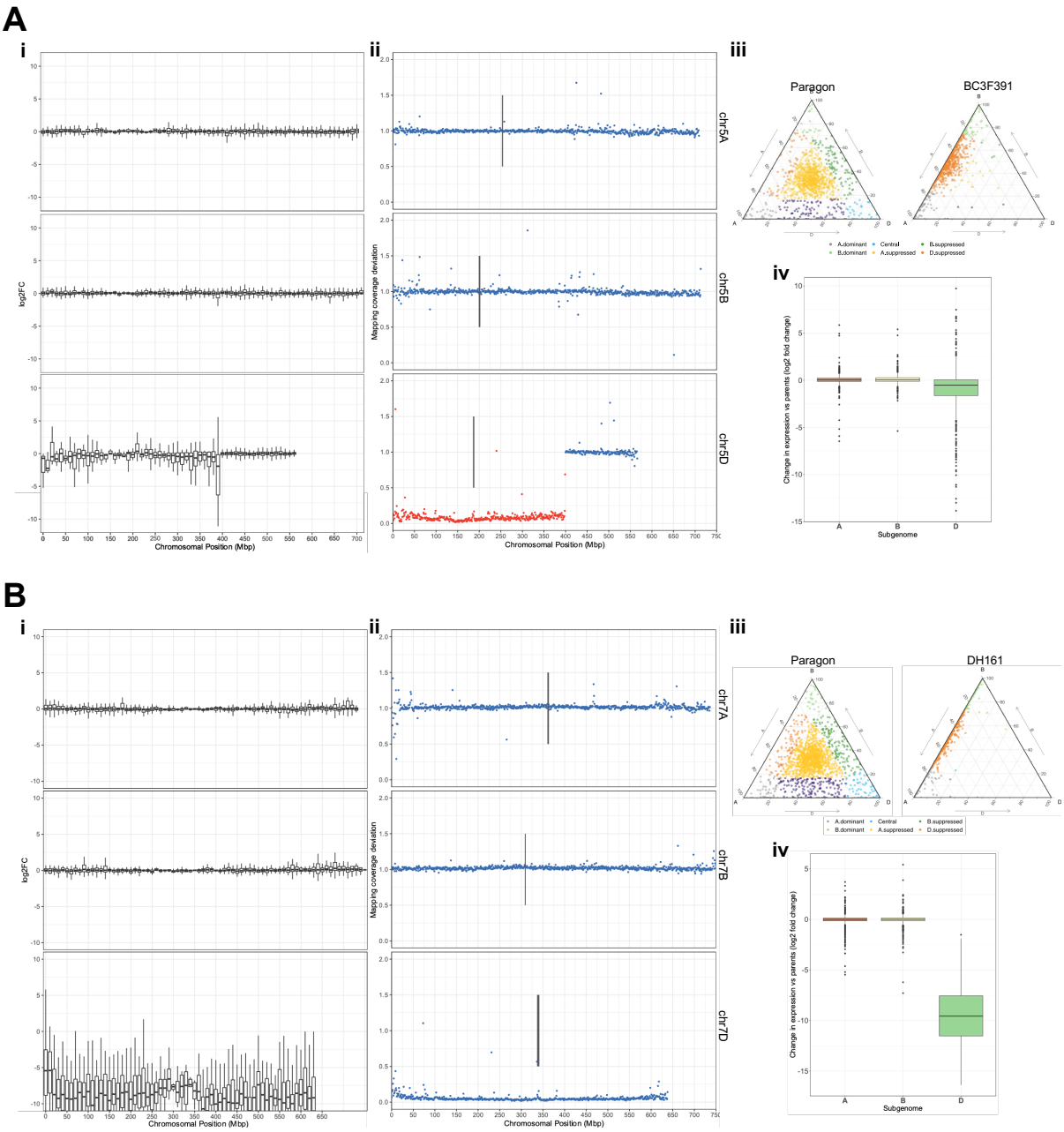

Fig. 4. Expression profile across introgressed and a deleted region and their homoeologous regions. Exploring triads **A** Within chr5D:1-400Mbp introgression in BC3F45 where chr5D copy is replaced with *Am. muticum* orthologue and **B** within chr7D in DH161 where the chr7D copy deleted. i. DESeq2 processed $\log_2$FC of expression compared to Paragon binned into 10Mbp windows ii. Macro level structure in 1Mbp windows. Each point represents the deviation in mapping coverage compared to the parent lines in 1Mbp windows across Chinese Spring RefSeq v1.0. Windows within assigned *Am. muticum* introgression blocks are coloured red; iii. Triad expression balance in triads where the D copy has been deleted or replaced by introgressed gene, comparing the wheat parent Paragon with the introgression line; iv. $\log_2$FC of A, B and D in triads in which the D copy has been deleted or replaced by an introgressed gene.

202

203 To complement the above approach and consider homoeologues whose expression may have changed but not
204 sufficiently to be called as significant by DESeq2, we looked at the log_2 fold change (log_2FC) in DESeq2
205 normalised expression counts. Plotting the log_2FC in 10Mbp windows across the chromosomes illustrates the
206 correlation between introgression boundaries and alteration of expression as well as a lack of general
207 expression change in the homoeologous regions. For the introgression and the deletion, we compared the
208 log_2FC of the A and B homoeologues of triads where the D copy had been introgressed or deleted with the
209 log_2FC of the A and B homoeologues of a control set of triads where the D copy is not differentially expressed
210 (fig 4A iv and 4B iv). We found no statistically significant difference between the test and control sets (two-
211 tailed t test p-values: deletion = 0.142; introgression = 0.0656). This indicates that, like the proportion of DEGs,
212 the change in expression counts of homoeologues in which the D copy has been downregulated/silenced does
213 not change beyond that expected by chance in triads in which the D copy is present and not differentially
214 expressed.

215 In lines possessing the chr5D introgression or the chr7D deletion, the balance of expression in the triads
216 shifted towards D suppression (fig. 4A iii), although this suppression was less extreme for the introgression due
217 to a partial compensation from the introgressed *Am. muticum* genes. Across chr5D:1-400Mbp, the region
218 introgressed in BC34F45, 66.4% of triads are balanced in Paragon, compared to just 1.56% of triads balanced in
219 the introgression line, with 74.4% being D suppressed. This further supports a lack of compensation as the
220 parental triad balance seen in the wheat parents is not retained, with triads that were balanced becoming D
221 suppressed and triads that were D suppressed remaining D suppressed.

222 To explore the indirect impact of expression on the wheat background caused by trans effects and not altered
223 copy number, we also looked at genes in genomic windows not deviating in coverage compared to the wheat
224 parent lines (fig. 3). Between 0.182% and 2.43% (107-1268 genes; 0.890% across all lines) of these wheat
225 genes were differentially expressed compared to the wheat parents. To assess whether any specific gene
226 functions were enriched in the differentially expressed genes we looked for enriched GO Terms (fig. S3). We
227 found some terms to be enriched, suggesting a non-stochastic impact on background transcription, however
228 differences between lines suggests that the nature of trans impact depends on the genes
229 introgressed/disrupted elsewhere in the genome. Some terms are enriched in more than 3 lines, suggesting
230 these are commonly affected in response to the large structural changes. These are oxidoreductase activity,
231 oxidation-reduction process, tetrapyrrole binding, catalytic activity, carbohydrate metabolic process, cofactor
232 binding, which are enriched in downregulated genes; and ion binding, hydrolase activity, and catalytic activity,
233 which are enriched in upregulated background genes.

234 Identifying candidate introgressed genes underlying Am. muticum derived rust resistance

235 Combining high resolution definition of segment positions with phenotypic information allows us to compare
236 lines and more accurately predict the location of genes underlying the phenotype of interest. Combining this
237 with a genome assembly of the introgressed wild relative allows us to identify introgressed genes that act as

238 candidate genes for the phenotype of interest. We explored this approach using previously reported rust
239 resistance phenotypes as a case study. Two of the lines that we sequenced, DH92 and DH121 (fig. 5), have
240 complete resistance at the seedling stage to Kansas isolates of *Puccinia striiformis tritici* (stripe/yellow rust)
241 (*17*). DH92 also displays chlorotic adult resistance to leaf rust and partial resistance to stem rust that is absent
242 in DH121. These lines have overlapping 5D segments, the positions of which were refined to 533.2-566.1Mbp
243 (32.9Mbp) in DH92, and 544.1-566.1Mbp (22Mbp) in DH121. The source of the stripe rust resistance is likely
244 within the overlapping 22.68Mbp region, and the source of leaf/stem rust resistance is likely within the
245 10.9Mbp region unique to DH92.

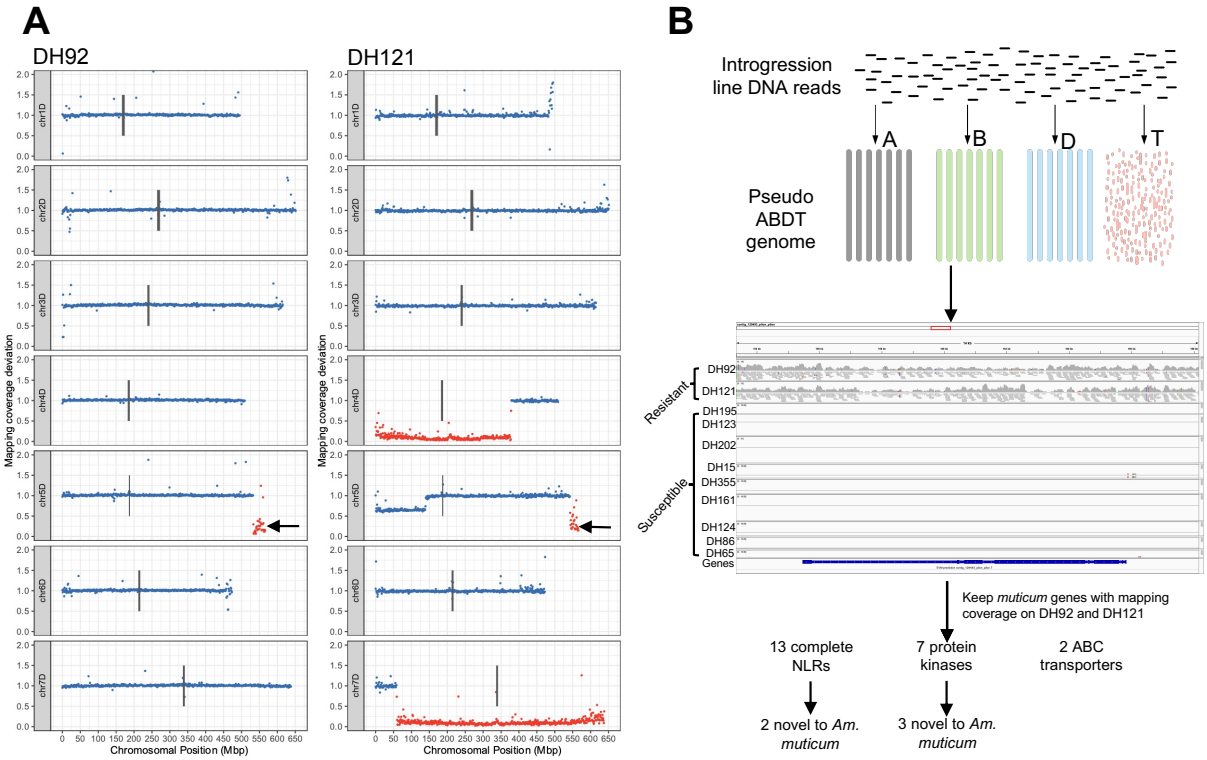

Fig. 5. Identifying candidate introgressed resistance genes. Introgression lines DH92 and DH121 possess a partially overlapping introgressed segment on chr5D, a common resistance phenotype to stripe rust but a differential resistance phenotype to leaf and stripe rust. A Macro-level structure of the D subgenome of DH92 and DH121 (no segments on A or B subgenomes). Each point represents the deviation in mapping coverage compared to the parent lines in 1Mbp windows across Chinese Spring RefSeq v1.0. Windows within assigned *Am. muticum* introgression blocks are coloured red. B Identifying resistance genes uniquely introgressed in DH92 and DH121 and thus candidates for the stripe rust resistance shared between the two lines.

246

247 Using a mapping-based approach to the pseudo ABDT genome and combining with functional annotation, we
248 identified 13 complete nucleotide-binding, leucine-rich repeat (NLR) immune receptors uniquely introgressed
249 in these two lines. 12 of these have a syntenic wheat orthologue within the overlapping region of the 5D
250 segments. 2 of the NLRs display unique NB-ARC domain signatures (< 80.0% protein identity) when compared
251 to 16 assembled wheat cultivars and wheat progenitor genomes; *Ae. tauschii*, *Triticum urartu*, and *T. turgidum*
252 ssp. *dicoccoides*. 10 of the NLRs are within a 597.34Kbp cluster, which includes the 2 NLRs with novel NB-ARC
253 domains, which are anchored within 19.06Kb from one another. We also identified 2 ABC transporters
254 uniquely introgressed, both of which have 5D orthologues with over 97.5% protein identity, and 7 protein
255 kinase genes uniquely introgressed. 6 of these are LRR protein kinases and 1 has a malectin-like domain and a

256 protein kinase domain. 3 of these protein kinases are highly diverged at the protein level compared to the
257 closest protein in wheat (52.2%, 74.2% and 77.0%). NLRs, ABC transporters and LRR protein kinases have all
258 been previously implicated in resistance to stripe, leaf and stem rust (*24–26*). Gene candidates are detailed in
259 table S6.

260 We identified 3 wall-associated protein kinases (WAKs), and 3 protein kinases uniquely introgressed in DH92
261 with orthologoues or proximal to orthologues of wheat genes in the 10.9Mbp non-overlapping region of the
262 5D segment. All but 1 of these were found on the same 104.7Kbp contig. 2 of the WAKs are orthologues of
263 TaWAK388 and TaWAK390 on 5D and 1 is orthologous to TaWAK255 on chr4A. Wall-associated kinases have
264 previously been associated with leaf rust adult plant resistance (APR) (*27*). Two of the protein kinases are
265 identical at the protein level and are most similar to TaWAK387 just upstream of the TaWAK388 and
266 TaWAK390. These may be truncated tandem duplications of this WAK. Unlike the other uniquely introgressed
267 genes identified, the WAKs have some reads mapping to them in most of the introgression lines but only in
268 DH92 is the coverage uniform across their lengths. This likely suggests that these are uniquely introgressed in
269 DH92 and thus can remain as resistance candidates, but similar *Am. muticum* WAKs present in other lines are
270 falsely mapping to these. This is supported by a lack of mapping across the rest of the contig in the other lines,
271 unlike DH92. Gene candidates are detailed in table S7.

272 Discussion

273 Using whole-genome sequencing to pinpoint wild relative introgressions in wheat – an affordable
274 approach to better characterise introgression lines

275 The current approach for studying synthetic introgression lines prior to deployment in breeding programmes
276 relies on cytogenetic and genotyping techniques, namely GISH and KASP (*12*, *18*). *De novo* discovery of SNPs to
277 produce higher density KASP markers has improved the resolution and as demonstrated here, recent KASP
278 genotyping was able to detect most of the introgressed segments identified with our approach. However,
279 these approaches lack the resolution needed to unpick the precise size and location of segments and will likely
280 miss small segments without the guidance of WGS data to identify areas in which additional markers should be
281 deployed. We observe this with the new chr6D segment, the small chr7D segment in DH195 and chr5D
282 segment in DH121, the latter two of which are novel sources of disease resistance.

283 We have demonstrated how whole genome sequencing data can be used to define introgressions to a very
284 high resolution as well as resolve large-scale structural changes in these lines. Downsampling has shown that if
285 we don't require SNP information, only 0.01x sequencing coverage is required to pinpoint the junctions of
286 known introgressed segments to a comparable resolution. Overlaying this information with KASP genotyping
287 will undoubtedly provide an affordable method to characterise sets of synthetic introgression lines more
288 accurately and comprehensively.

289 Introgressed segments nested within complex genomic structures, such as in DH202 (fig. S1), can only be
290 inferred in conjunction with cytogenetic data and/or segregation patterns of DH pairs. In this example, the
291 part of the introgression signal from chr7D appears on chr7A instead, due to a 7D-7A translocation. Some
292 introgression segment boundaries, such as the left-hand border of chr2A in DH15, can be identified but are
293 difficult to pinpoint precisely due to structural complexities around the junction. Therefore, caution is advised
294 when relying on introgression assignments provided by WGS data alone, particularly for complex lines with
295 several large introgressions/deletions/duplications. However, for most lines, where genomic structure is
296 simpler, this approach is robust, and is nevertheless an improvement on lower resolution methods, even if
297 only to identify confounding structural complexities that would otherwise have been missed.

298 We have found that crossover points between wheat and *Am. muticum* mostly take place within or adjacent to
299 genes. Previous work has shown crossovers between wheat and wild relatives are enriched in gene rich
300 regions (*28*), which mirrors recombination rates along the genome (*29*). Here we have achieved sufficient
301 resolution to reveal these wild relative crossovers are taking place not only in regions of open chromatin and
302 increased recombination rate, but within the genes themselves. This may be because these are the points at
303 which synteny is sufficiently high for recombination to take place.

304 Genomic instability following alien introgression crossing

305 We have illustrated that structural disruption is common in introgression pre-breeding material, including
306 homoeologous pairing and recombination, and duplications and deletions up to chromosome size. This is likely
307 caused by the *Am. muticum*-induced suppression of the *Ph1* locus which is currently used to induce
308 recombination between wheat and wild relative chromosomes. This *Ph1* suppression enables pairing of
309 chromosomes from different subgenomes, which can cause translocations between subgenomes and unstable
310 chromosome pairings that can cause large deletions and duplications. Forced pairings between wheat and wild
311 relative chromosomes in the F1 cross are likely also responsible for structural change. The DH process could be
312 inducing structural change, but the fact we see this in lines that haven't undergone this process excludes the
313 DH process from being the primary explanation. We can be confident that *Ph1* is contributing to the structural
314 change due to the evidence of subgenome pairings we see tied to some of these chromosomal aberrations.
315 Backcrossing in the development of these lines will have removed much of the initially induced structural
316 change, so what we see here is a subset of structural change initially generated. An awareness of
317 chromosomal aberrations is important for breeders using these lines in their breeding programmes. It will be
318 important to identify the location of the *Ph1* suppressor in *Am. muticum* and other wild relatives that have an
319 innate *Ph1* suppression system, such as *Ae. speltoides* (*30*) to prevent segments being carried forward into
320 breeding programmes that contain a *Ph1* suppressor that could generate further genomic disruption.

321 Smaller scale variation in mapping coverage suggests that structural disruption is not restricted to large
322 crossovers and provides some evidence of many potentially smaller scale structural variations in these lines
323 that we can't accurately assess with our available data, such as transposable element mobilisation and smaller

324 INDELs. It will be important to assess the nature and extent of such variation in the future. To understand this
325 type of variation, we will need a genome assembly of an introgression line and the wheat parents used in the
326 cross, or a genome assembly of the wheat parent and long read data from the introgression line like we
327 produced here for DH65. Unfortunately, structural variation between available chromosome-level genome
328 assemblies and Paragon and Pavon76 is too great for structural variants arising from genome shock to be
329 distinguished from existing structural variation between the cultivars.

330 Given that we see large-scale structural change as a by-product of most synthetically derived introgressions,
331 perhaps similar structural changes have been induced from historic natural introgressions of wild relative
332 material. We are increasingly becoming aware of the abundance of introgressions throughout wheat
333 germplasm (*31*, *32*); it is possible that many of the structural changes/rearrangements we see in wheat
334 accessions has its origin in unstable chromosome pairings induced by natural introgression events and could
335 be driving the evolution of wheat genomes beyond the addition of novel genes.

336 Gene expression following alien introgression, lack of homoeologous balancing, and impact on the 337 wheat transcriptome

338 Many of the introgressed genes are differentially expressed compared to the wheat orthologue replaced. This
339 makes sense biologically due to the very different genomic background the *Am. muticum* genes have been
340 introgressed into, with many factors likely underlying these observed differences such as mismatches between
341 transcription factor binding sites of *Am. muticum* genes and the transcription factors found in wheat. Two
342 previous studies have explored the expression of genes in wheat introgression lines with barley (*33*) and
343 *Aegilops longissima* (*34*) introgressed. Due to the differences in methods used for different studies, it is
344 difficult to compare the total proportion of DEGs. However, both previous studies also show that many
345 introgressed genes are differentially expressed with most of these being downregulated or silenced.

346 We expected to see some balancing of expression in the homoeologues of genes heavily downregulated or
347 silenced due to introgression or deletion events, but we didn't observe significant alteration in the expression
348 of homoeologues. This lack of response suggests that if large-scale balancing of triad expression does take
349 place, it must require selection pressure, which these synthetic lines lack. Now that genome assemblies are
350 available for wheat cultivars possessing many wild relatives introgressions (*31*) that have undergone extensive
351 artificial selection in a wheat background, it will be interesting to analyse how these introgressed regions are
352 expressed and whether balancing of triad expression arises after a period of selection.

353 Due to the complex nature of the introgression line genomes, it is difficult to distinguish between the effect of
354 introgressions and deletions/monosomies on the background expression. In the future, analysing the
355 expression of introgression lines with less complex genomes may allow us to better unpick the trans-
356 regulatory effects of introgressed genes from those of deleted or duplicated wheat genes. We see some
357 commonly enriched GO Terms in the genomic background that may be linked with cellular stress or loss of

358 cellular homeostasis; this conclusion is supported by conclusions drawn in the wheat/barley introgression line
359 (*33*). The lines without these enriched GO Terms have less disruption overall, with fewer differentially
360 expressed genes in the background and thus may either not have sufficient genomic stress to trigger these
361 responses or lack sufficient sample size of DEGs to call significance.

362 A case study for uncovering candidate introgressed genes underlying phenotypes of interest

363 Combining high resolution detection of introgressed segment borders with phenotype information and a genic
364 assembly of *Am. muticum* has enabled us to identify likely regions for novel resistances and produce lists of
365 candidate genes. This will allow breeders to target regions to incorporate into elite lines and to analyse further
366 to identify causal resistance genes. It also acts as a template that can be built upon for new methods to unpick
367 traits of interest in sets of introgression lines.

368 We identified the probable region of stripe rust resistance in DH92 and DH121 as being within the 22.68Mbp
369 overlapping region of the chr5D segment. The small size and telomeric position of this segment makes it
370 conducive for use in breeding. Within this region, we have identified candidate resistance genes, including 3
371 novel NLRs and 3 novel LRR Pkinase proteins. We searched for other classes of genes that have been cloned
372 for stripe rust resistance (*35*), such as hexose transporter, wheat Kinase-START (WKS), tandem kinase-
373 pseudokinase (TKP), but found no examples of these genes uniquely introgressed in these lines. The DH92
374 resistance to leaf rust that is not shared with DH121, is only seen in adult plants and to a composite of isolates;
375 this race non-specific APR tends to be more durable and, in combination with the small segment size, makes
376 this resistance another good target for further characterisation. We identified 3 WAKs and 3 protein kinases
377 uniquely introgressed in DH92. Wall-associated kinases have previously been shown to confer resistance to
378 leaf rust that looks similar to APR (*27*) and protein kinase proteins, such as Yr36, have been implicated in APR
379 (*36*). It should be noted that any resistance here could be conferred by genes that are absent from the
380 assembly or the annotation. If only interested in either the stripe rust or leaf/stem rust resistance, DH92 and
381 DH121 could be crossed to recover the desired resistance in a smaller segment with less linkage drag.

382 Accession-level differences between wild relatives used for introgression crossing might underlie differences in
383 phenotype between introgression lines with overlapping segments. This is likely the case for the leaf rust
384 resistance in DH195. DH195 has seedling and adult leaf rust resistance not seen in DH202, DH123, or
385 DH121(*17*), all of which have 7D/7T segments. Differences in segment size and position between these lines
386 (fig. S1) are insufficient to explain the differential resistance we see as there is no segment in DH195 with no
387 overlaps with the other 3 lines. However, the *Am. muticum* accession used to produce DH195 and DH202 (*Am.*
388 *muticum* 2130004) is different to that used to produce DH121 and DH123 (*Am. muticum* 2130012) so
389 differences in resistance genes between these accessions in the 16.69Mbp region at the end of the
390 chromosome may underlie resistance. Isolating this telomeric segment from the other DH195 segment and
391 screening for resistance will be able to confirm this and provide a new segment conferring resistance for

392 breeders to utilise. Due to the *Am. muticum* assembly being produced from *Am. muticum* 2130012, any
393 resistance genes specific to 2130004 would not be present in the assembly and so cannot be assessed.

394 These lines as well as many other sets of synthetic introgression lines are being phenotyped for a variety of
395 agronomically important traits and genome assemblies for additional wild relatives are likely to be produced in
396 the coming years. The analysis we have described here will work better with improved assemblies in which
397 contiguous introgressed segments can be reconstructed and introgressed content fully assessed. This study
398 provides a schematic that can be followed to characterise introgression lines, identify likely positions of genes
399 of interest within segments and candidate genes underlying the phenotype. This will facilitate more effective
400 utilisation of introgression pre-breeding material in wheat breeding programmes.

401 Materials and Methods

402 Introgression line production and selection

403 As described in (*11*, *12*), *Am. muticum* accessions 2130004/2130012 were crossed with Pavon76 or Chinese
404 Spring. The F1 interspecific hybrid was backcrossed 3 times, once with Paragon, Pavon76 or Chinese Spring
405 and twice with Paragon. To make homozygous lines in which introgressions are stably inherited, the resulting
406 BC3 lines were either pollinated with maize and treated with colchicine to generate doubled haploids (DH) (*12*)
407 or were selfed 2 or 3 times. 13 DH lines, 3 selfed lines and 1 heterozygous BC line, along with *Am. muticum*,
408 Paragon, Pavon76 and Chinese Spring, were selected for DNA WGS. 12 of the lines belong to a pair or a trio of
409 lines that derive from seed from the same BC1 cross, so common segments are not independently derived. 4
410 DH and 2 BC lines, along with *Am. muticum*, Paragon, Pavon76 and Chinese Spring, were selected for RNA
411 extraction and sequencing.

412 WGS, read processing, mapping and SNP calling:

413 *Am. muticum* introgression lines and wheat parents were grown in a growth room (16h, 21°C day/8h, 18°C
414 night). Genomic DNA from young leaves was isolated using extraction buffer (0.1 m Tris–HCl pH 7.5, 0.05 m
415 EDTA pH 8.0, 1.25% SDS). Samples were incubated at 65 °C for 1 h before being placed on ice and mixed with
416 ice-cold 6 m NH4C2H3O for 15 min. The samples were then spun down, the supernatant was mixed with
417 isopropanol to pellet the DNA and the isolated DNA was treated with RNase A then purified with
418 phenol/chloroform. DNAs were dissolved in TE (10mM Tris-HCl pH8.0, 0.1mM EDTA). PCR-free libraries were
419 produced from this DNA with >600bp insert sizes (gel size-selection). These were sequenced on Illumina
420 NovaSeq 6000 S4 flowcells to produce 150bp paired-end reads. Adaptors were removed and reads trimmed
421 for quality using Trimmomatic (*37*) with the following parameters: ILLUMINACLIP:TruSeq3-PE-2.fa:2:30:10
422 SLIDINGWINDOW:4:15 MINLEN:40 CROP:150. Contaminants were screened and removed using Kontaminant
423 (*38*) with *E. coli*, phage, and vector libraries.

424 The cleaned reads were mapped to the Chinese Spring reference genome RefSeqv1.0 (*39*) using BWA-MEM
425 (*40*) with the -M parameter to enable duplicates to be marked. The alignment was filtered using samtools (*41*):
426 supplementary alignments, improperly paired reads, and non-uniquely mapped reads (q <= 10) were removed.
427 PCR duplicates were detected and removed using Picard's MarkDuplicates (*42*). Variants were called using
428 samtools mpileup (*41*) and bcftools call (*43*) using the multiallelic calling model -m.

429 Initial variant filtering was performed using GATK VariantFiltration (*42*) to remove INDELs and to retain SNPs
430 with a quality score >= 30 and a read depth >= 10 for the parental lines and >= 5 for the introgression lines.
431 Introgression line SNPs were further filtered as follows: homozygous SNPs were kept if 5 or more reads
432 supporting the alternative allele and the allele frequency (AF) was 1; heterozygous SNPs were kept if 3 or more
433 reads supporting each allele. Sites with more than 3 alleles were removed.

434 In silico karyotyping - calculating mapping coverage deviation compared to wheat parents

435 The number of mapped reads post filtering and duplicate removal was counted across genomic windows
436 (1Mbp and 100Kbp) in RefSeq v1.0 using bedtools makewindows (*44*) and hts-nim-tools (*45*) for the wheat
437 parents (Chinese Spring, Paragon and Pavon76) and each introgression line. Mapped read counts were
438 normalised by dividing by the total read number post duplicate removal. Normalised counts of each
439 introgression line were divided by the normalised count of each wheat parent in its crossing history (Paragon +
440 Pavon76 or Paragon + Chinese Spring) and the number closest to 1 was kept as the coverage deviation for that
441 window, under the assumption that the parent with mapping coverage closest to the introgression line is the
442 parental donor in that window. The resulting number reflects the copy number of wheat DNA in that window
443 relative to the wheat parent. A number of 1 indicates that the DNA in that window is present in the same
444 amount as in the parent line. A number approaching 0 suggests either a deletion or an introgression has
445 occurred at that region, and a number of 2 suggests a duplication event has taken place. Intermediate values
446 indicate a heterozygous copy number change. We defined windows with a coverage deviation between 0.8
447 and 1.2 as being 'normal' and not in copy number variation compared to the wheat parents.

448 Identifying *Am. muticum*-specific SNPs and assigning introgressed regions:

449 A set of custom python scripts were used to analyse the coverage deviation files and vcfs and identify the
450 introgression segments in each line. These scripts, alongside more detailed methods, are available at:
451 https://github.com/benedictcoombes/alien_detection. First, we produced 18,496,474 SNPs between *Am.*
452 *muticum* and Chinese Spring that weren't shared with either Paragon or Pavon76. *Am. muticum* SNPs were
453 retained as genome-specific if not shared with Paragon or Pavon76. At heterozygous sites where one allele
454 was specific to *Am. muticum*, the specific SNP was retained. If two alternative alleles present, both were kept if
455 both were specific to *Am. muticum*.

456 Introgression line SNPs were then assigned as *Am. muticum* if matching a muticum specific SNP in position and
457 allele. Sites exceeding 3x mean coverage level were removed; this is a signature of collapsed repeat expansion.

458 These SNPs were then split into homozygous and heterozygous and binned into 1Mbp windows using bedtools
459 coverage (*44*). Coverage deviation blocks were defined based on contiguous blocks of 1Mbp windows with
460 coverage deviation < 0.7, with windows within 5Mbp from the previous coverage deviation block being
461 merged. The block was discarded if < 80.0% of constituent windows had a coverage deviation < 0.7. 1Mbp
462 windows containing >= 55 homozygous *Am. muticum* specific SNPs and a ratio of homozygous to heterozygous
463 *Am. muticum* specific SNPs >= 4 that fell within a coverage deviation block were classified as candidate *Am.*
464 *muticum* windows. Coverage deviation blocks with >= 14% windows assigned as *Am. muticum* using the
465 parameters above were classed as an introgressed segment. These parameters are adjustable and were
466 chosen because they revealed previously known introgression segments and didn't falsely class any known
467 deletions as introgressions. The coverage deviation values in the 100Kbp windows up and downstream of
468 either end of the introgression blocks were examined to determine where the coverage deviation starts to
469 decrease. The first 100Kbp window either side that falls below coverage deviation of 0.7 was assigned as the
470 border window of the segment. To locate the precise position of this junction, the BAM alignment files for *Am.*
471 *muticum*, Paragon, Pavon76 and the introgression line were loaded into IGV (*46*). The border window (+-
472 100Kbp) identified above was searched manually to find the position where the coverage and SNP profile
473 switches from that of the wheat parents to that of *Am. muticum*.

474 ## KASP validation

475 Genomic DNA was isolated from leaf tissue of 10-day old seedlings in a 96-well plate as described by Thomson
476 and Henry (*47*). All DH lines were genotyped alongside the three parental wheat genotypes (Chinese Spring,
477 Paragon and Pavon 76) and the two *Am. muticum* accessions as controls. For each KASP™ assay, two allele-
478 specific primers and one common primer were used (Table S1). The genotyping procedure was as described in
479 (*48*). In summary, the genotyping reactions were set up using the automated PIPETMAX® 268 (Gilson, UK) and
480 performed in a ProFlex PCR system (Applied Biosystems by Life Technology) in a final volume of 5 µl with 1 ng
481 genomic DNA, 2.5 µl KASP reaction mix (ROX), 0.068 µl primer mix and 2.43 µl nuclease free water. PCR
482 conditions were set as 15 min at 94°C; 10 touchdown cycles of 10 s at 94°C, 1 min at 65–57°C (dropping 0.8°C
483 per cycle); and 35 cycles of 15 s at 94°C, 1 min at 57°C. Fluorescence detection of the reactions was performed
484 using a QuantStudio 5 (Applied Biosystems) and the data analysed using the QuantStudio™ Design and Analysis
485 Software V1.5.0 (Applied Biosystems).

486 ## Nanopore junction validation

487 DNA from introgression line DH65 extraction was prepared using ligation sequencing kit SQK-LSK109 and
488 sequenced on a MinION using the R9.4.1_RevD flow cell. Reads were filtered using NanoFilt (*49*) to remove
489 reads below a quality score of 7 or a length of 1Kbp. Filtered reads were mapped to RefSeq v1.0 using
490 minimap2 (*50*) with parameters -ax map-ont and --secondary=no. Mapped reads around the breakpoint
491 (chr4D:51283000-51595000) were extracted using samtools (*41*), including clipped portions of mapped reads,
492 and assembled using wtdbg2 (*19*). The resulting contigs were mapped to RefSeq v1.0 using minimap2 (*50*) with

493 parameters -ax map-ont and examined in IGV (*46*) along with the mapped illumina reads from the parent lines
494 and DH65.

495 ## Genome assembly of Am. muticum:

496 DNA from *Aegilops mutica* (now *Am. muticum*) line 2130012 (JIC) was prepared using ligation sequencing kit
497 SQK-LSK109 and sequenced on a MinION using the R9.4.1_RevD flow cell. 178Gbp of raw nanopore reads were
498 filtered using NanoFilt (*49*), removing reads below a quality score of 7 or a length of 1Kbp. Filtered reads were
499 assembled using the Flye assembler (*20*). Following nanopore read polishing integrated into Flye, we
500 conducted 2 rounds of pilon (*51*) polishing using 102Gbp of illumina short reads to correct systematic errors in
501 the nanopore data. Finally, haplotigs that were not collapsed in the assembly were detected and resolved
502 using purge_haplotigs (*52*). Gene completeness was assessed using BUSCO 3.0.2 (*22*) with parameters -l
503 viridiplantae_odb10 –species wheat and -m geno.

504 ## Estimating genome size:

505 Filtered nanopore reads were mapped back to the polished genome assembly using minimap2 (*50*) with
506 parameters -x asm5 and filtered to retain uniquely mapping reads with mapQ >= 10. We computed mean
507 coverage across single-copy genes in the assembly. These were identified by orthofinder (*53*) with *T. aestivum*,
508 *T. turdigum*, *Ae. tauschii*, *T. urartu*, *Brachypodium distachyon*, and *Arabidopsis thaliana*. *Am. muticum* genes
509 belonging to an orthogroup with no other *Am. muticum* genes in all species represented at least once and
510 fewer than 20 total genes in the orthogroup, were used. The estimated genome size was calculated as the
511 total number mapped bases / mean coverage across single-copy genes, using post-filtering numbers.

512 ## Repeat annotation:

513 A de novo library of transposable elements was produced using EDTA v1.9.5 (*54*), using cds sequences from *T.*
514 *aestivum* to exclude protein-coding regions from the library. The resulting library was aligned to the assembly
515 using blastn (*55*) and sequences with fewer than 3 full length hits (defined as over 80.0% similarity across more
516 than 80.0% of the length of the element) were removed and remaining sequences were clustered using cd-hit-
517 est v4.6.7 (*56*) with parameters aL 0.8 aS 0.8 -c 0.8 to remove redundant sequences. The resulting library was
518 used to mask the genome assembly using RepeatMasker v4.07 (*57*) with parameters -s -no_is -norna -nolow -
519 div 40 -cutoff 225.

520 ## Gene annotation:

521 *Ab initio*, protein homology and transcriptome evidence were combined to predict protein-coding genes in the
522 *Am. muticum* assembly. First, the *Am. muticum* RNA reads (4 root replicates and 4 shoot replicates) were
523 trimmed using Trimmomatic (*37*) with the parameters ILLUMINACLIP:BBDUK_adaptor.fa:2:30:12
524 SLIDINGWINDOW:4:20 MINLEN:20 AVGQUAL:20. The trimmed RNA reads were mapped to the masked

525 genome using STAR (*58*). Transcripts were assembled using four independent reference-guided approaches;
526 Trinity (*59*); StringTie (*60*), cufflinks (*61*) and CLASS2 (*62*). Transdecoder (*63*) was used on each set of
527 transcripts to produce coding ORFs. PORTCULLIS (*64*) was used to produce splice information. Uniprot (*65*)
528 reference proteomes for *T. aestivum*, *Ae. tauschii*, *T. turgidum*, *Oryza sativa*, *B. distachyon*, and *A. thaliana*
529 were aligned to the genome using blastx (*55*). Mikado (*66*) was used to merge and refine the transcripts
530 produced by each tool, aided by the splice site information and the protein homology evidence. The same
531 uniprot reference proteomes as above were aligned to the masked genome using TBLASTN (*55*). Hits with an
532 e-value below 1e-5 and sequence identity greater than 75% within 20Kb were merged using bedtools merge
533 (*44*). These regions were searched using exonerate (*67*) to refine protein alignments. To produce a set of
534 transcript annotations to train Augustus (*68*), Mikado protein coding genes were filtered to retain multi-exon
535 genes with < 80.0% amino acid identity with any other protein, not have a stop codon in the ORF, and be at
536 least 500bp away from another gene. Of the remaining transcripts, the 2000 with the highest mikado score
537 were retained and randomly split into 1800 training genes and 200 testing genes. The AUGUSTUS HMM was
538 trained using these transcripts using etraining followed by 10-fold cross validation using optimize_augustus.pl.
539 To produce initial *ab initio* gene predictions, Augustus was run using this HMM, along with intron hints
540 produced from the STAR bam file using bam2hints from Augustus. EvidenceModeler (*69*) was used to produce
541 a set of HC gene models with *ab initio*, transcriptome, and protein homology evidence. This set of HC genes
542 was used to retrain Augustus as before, as well as GlimmerHMM (*70*). Augustus, SNAP (*71*) (using the rice
543 HMM) and GlimmerHMM were run to produce final ab initio gene predictions. These predictions were
544 incorporated with the transcript and protein homology evidence using EvidenceModeler to produce final gene
545 models with the following weightings: mikado transcriptome, weight 14; Augustus gene models - weight 4;
546 exonerate protein evidence - weight 7; SNAP gene models - weight 1; GlimmerHMM gene models - weight 2.
547 Predicted proteins blasted to the TREP database of transposable elements and to TREMBL proteins. Proteins
548 were retained with no significant hit to TREP (*72*) but at least one significant hit to TREMBL (*73*). Gene
549 functions were assigned using eggnog 5.0 (*74*).

550 ## Assigning orthologue pairs:

551 *Am. muticum*/wheat orthologue pairs were assigned using best reciprocal blast hits between *muticum* and
552 each wheat subgenome independently. *Am. muticum* proteins (extracted and translated from gff) and wheat
553 proteins (taken from IWGSC 1.1 pep.fa file for wheat proteins) were aligned reciprocally using blastp (*55*) with
554 parameters -outfmt 6 -max_hsps 3 -max_target_seqs 3 -evalue 1e-6. Hits were retained if percentage identity
555 >= 80.0% and alignment length was >= 50.0% query length. An orthologue pair was defined as a pair of
556 proteins whose top hit were each other.

557 ## Classifying introgressed genes

558 RefSeq v1.0 genome and the draft *Am. muticum* assembly were concatenated to form a pseudo ABDT genome.
559 DNA reads from the introgression lines were mapped to this genome and filtered using the same process as

560 mapping to RefSeq v1.0 alone. Introgressed *Am. muticum* genes in each line were defined as those with a
561 wheat orthologue with a start position that fell within a region labelled as a *Am. muticum* introgression and >=
562 2x mean mapping coverage across its length from the ABDT pseudo genome mapping above.

563 ## mRNA extraction, sequencing, alignment, and quantification

564 Seeds were germinated and grown to the 4th leaf stage in a growth chamber set to 22C, 16-hour days. Plants
565 were well watered and supplemented with nutrients. The 4th leaf was extracted and snap frozen in liquid
566 nitrogen within 20 seconds of sampling and stored at -80C. Three reps of each line were sampled individually.
567 Each sample was ground in a pestle and mortar using liquid nitrogen and a sub-set taken for Total RNA
568 extraction using Qiagen RNeasy plant mini kit (Qiagen, Germany). DNA was removed using a digestion step
569 with RNase-free DNase (Qiagen, Germany). Ratios of 260:280 were measured using a Nanodrop (ThermoFisher
570 Scientific) and samples were only used with ratios between 1-9 and 2.1. Only samples with RNA integrity
571 number (RIN) >8 and a concentration of 50-200ng/ul (Agilent Bioanalyzer) were sequenced.

572 Library preparation was conducted using automated NEBNext Ultra II Directional RNA-Seq library construction
573 with Poly-A selection and was sequenced in triplicate on an Illumina NovaSeq 6000 S2 flowcell by Genomic
574 Pipelines at the Earlham Institute to produce 150bp paired-end reads. RNA reads were trimmed using
575 Trimmomatic (*37*) with the parameters ILLUMINACLIP:BBDUK_adaptor.fa:2:30:12 SLIDINGWINDOW:4:20
576 MINLEN:20 AVGQUAL:20. The gff3 for the high confidence CS genes was concatenated with the gff3 for *Am.*
577 *muticum* genes. Splice site hints for HISAT2 were produced using extract_splice_sites.py from HISAT-2.0.4 (*75*).
578 The trimmed reads were mapped to the pseudo ABDT genome using HISAT2 with the splice hint file provided
579 and parameters -k 101 --dta --rna-strandness RF. Non uniquely mapping reads were removed using samtools
580 view -q 40. Stringtie (*60*) was used to compute gene-level abundances, outputting both raw counts and
581 transcript-per-million (TPM) values.

582 ## Differential expression analysis:

583 For each wheat gene in a region identified as introgressed, they were either removed or their expression count
584 was replaced with that of its *Am. muticum* orthologue. Differential expression analysis between each
585 introgression line and its two wheat parents was performed using DESeq2 (*23*). A gene was considered to be
586 differentially expressed if it had an adjusted p-value below 0.05 and an absolute $\log_2$FC >= 1 in both parental
587 comparisons. Differentially expressed genes were partitioned into those in introgressed regions, deleted
588 regions, duplicated regions, and in the unaffected background where coverage deviation is between 0.8 and
589 1.2.

590 ## Testing triad expression balancing

591 To examine whether genes belonging to triads that have homoeologues that have been replaced by a *Am.*
592 *muticum* gene or have been deleted, we took a test set of triads (*76*) that satisfied the following conditions:

593 the D copy is introgressed or deleted and called as downregulated; the A and B copy are in normal copy
594 number regions (coverage deviation between 0.8 and 1.2); and all homoeologues have normalised expression
595 count across samples >= 1. These were compared to control sets of triads that satisfied the same conditions
596 except the D copy was not called as differentially expressed and had abs(log_2FC) <= 0.20. These sets were used
597 for both the comparison of number of triads with A and/or B homoeologue upregulated and for the
598 comparisons of the mean log_2FC of the A and B homoeologues between the test and control sample of triads.
599 The significance of these comparisons was tested using two-tailed Fisher's exact test and two-tailed t test,
600 respectively.

601 ## GO Term analysis

602 We transferred functional GO Term annotation from genes in the RefSeq v1.0 annotation to genes in the
603 RefSeq v1.1 annotation if they shared greater that 99% similarity across greater than 90.0% of their length.
604 Statistically enriched GO Terms within the differentially expressed background gene set were computed using
605 the R package topGO (*77*) with the following parameters: nodeSize=10; classicFisher test $p < 0.05$ and
606 algorithm="parentchild". Enrichment for GO Terms involved in biological processes was tested against all
607 background genes that fall within windows with mapping coverage deviation between 0.8 and 1.2. Bubble
608 plots were plotted using adapted code.

609 ## Identifying introgressed resistance genes:

610 *Am. muticum* NLR genes were identified using two parallel methods. The first was to scan the gene models for
611 typical NLR domains using hmmscan from the HMMER package (*78*) in the filtered protein-coding gene models
612 produced by EVM. The second was to scan the entire genome de novo for complete, functional NLR protein-
613 coding regions using NLRAnnotator (*79*). This allowed several additional NLR genes whose gene model had
614 been filtered out or was never constructed to be recovered. Other types of genes that have been previously
615 implicated in stripe rust resistance (*35*) (ABC transporters, Pkinases, hexose transporters, wheat Kinase-START
616 genes, tandem kinase-pseudokinase proteins) were identified from the eggnog annotation and validated
617 manually using hmmscan and pfam domains. Resistance genes were manually checked using IGV to identify
618 candidates with even sequencing coverage across the genes in DH92 and DH121 only, in the case of the shared
619 stripe rust resistance, and across the genes in DH92 only, in the case of the DH92-specific leaf and stem rust
620 resistance. To reduce the number of genes to manually check, we removed any genes with less than 2x mean
621 mapping coverage across their length in either DH92 or DH121. The gene models were manually curated using
622 the available evidence. For NLR predictions with no gene model but transcriptomic and ab initio evidence,
623 gene models were manually constructed. The novelty of the uniquely introgressed NLRs was tested by
624 extracting the NB-ARC domains using hmmscan and aligning them using blastp to the proteins of HC genes
625 from 10 wheat cultivars, and to the proteins of the wheat progenitor species: *Ae. tauschii*; *T. urartu*; and
626 *T. turgidum* ssp. *dicoccoides*. Hits below 85% identity were considered novel. The novelty of the other protein

627 types was tested by aligning the whole amino acid sequence to the same protein set; proteins below <80.0%
628 were considered novel.

629 ## References

630 1. M. Reynolds *et al.*, Achieving yield gains in wheat. *Plant Cell Environ.* **35**, 1799–1823 (2012).

631 2. M. Hao *et al.*, The resurgence of introgression breeding, as exemplified in wheat improvement. *Front.*
632 *Plant Sci.* **11**, 252 (2020).

633 3. G. Charmet, Wheat domestication: lessons for the future. *C R Biol*. **334**, 212–220 (2011).

634 4. J. J. Valkoun, Wheat pre-breeding using wild progenitors. *Euphytica*. **119**, 17-23 (2001).

635 5. D. K. Ray, N. D. Mueller, P. C. West, J. A. Foley, Yield trends are insufficient to double global crop
636 production by 2050. *PLoS One*. **8**, e66428 (2013).

637 6. G. Doussinault, A. Delibes, R. Sanchez-Monge, F. Garcia-Olmedo, Transfer of a dominant gene for
638 resistance to eyespot disease from a wild grass to hexaploid wheat. *Nature*. **303**, 698–700 (1983).

639 7. B. Friebe, K. S. Gill, N. A. Tuleen, B. S. Gill, Transfer of Wheat Streak Mosaic Virus Resistance from
640 *Agropyron intermedium* into Wheat. *Crop Sci*. **36**, 857–861 (1996).

641 8. A. M. Fatih, Analysis of the breeding potential of wheat-Agropyron and wheat-Elymus derivatives. I.
642 Agronomic and quality characteristics. *Hereditas*. **98**, 287–295 (1983).

643 9. E. R. Sears, *The transfer of leaf-rust resistance from Aegilops umbellulata to wheat.* (1956).

644 10. D. L. Klindworth *et al.*, Introgression and characterization of a goatgrass gene for a high level of
645 resistance to ug99 stem rust in tetraploid wheat. *G3 (Bethesda)*. **2**, 665–673 (2012).

646 11. J. King *et al.*, A step change in the transfer of interspecific variation into wheat from Amblyopyrum
647 muticum. *Plant Biotechnol. J.* **15**, 217–226 (2017).

648 12. J. King *et al.*, Development of Stable Homozygous Wheat/Amblyopyrum muticum (Aegilops mutica)
649 Introgression Lines and Their Cytogenetic and Molecular Characterization. *Front. Plant Sci.* **10**, 34
650 (2019).

651 13. S. Khazan *et al.*, Reducing the size of an alien segment carrying leaf rust and stripe rust resistance in
652 wheat. *BMC Plant Biol.* **20**, 153 (2020).

653 14. M.-D. Rey *et al.*, Exploiting the ZIP4 homologue within the wheat Ph1 locus has identified two lines
654 exhibiting homoeologous crossover in wheat-wild relative hybrids. *Mol. Breed.* **37**, 95 (2017).

655 15. A. C. Martín, M.-D. Rey, P. Shaw, G. Moore, Dual effect of the wheat Ph1 locus on chromosome synapsis
656 and crossover. *Chromosoma*. **126**, 669–680 (2017).

657 16. D.-H. Koo, B. Friebe, B. S. Gill, Homoeologous recombination: A novel and efficient system for
658 broadening the genetic variability in wheat. *Agronomy*. **10**, 1059 (2020).

659 17. J. P. Fellers *et al.*, Resistance to wheat rusts identified in wheat/ *Amblyopyrum muticum* chromosome
660 introgressions. *Crop Sci* (2020), doi:10.1002/csc2.20120.

661 18. S. Grewal *et al.*, A novel approach to develop wheat chromosome-specific KASP markers for detecting
662 Amblyopyrum muticum segments in doubled haploid introgression lines. *BioRxiv* (2021),
663 doi:10.1101/2021.09.29.462370.

664 19. J. Ruan, H. Li, Fast and accurate long-read assembly with wtdbg2. *Nat. Methods*. **17**, 155–158 (2020).

665 20. M. Kolmogorov, J. Yuan, Y. Lin, P. A. Pevzner, Assembly of long, error-prone reads using repeat graphs.
666 *Nat. Biotechnol.* **37**, 540–546 (2019).

667 21. J. Pellicer, I. J. Leitch, The Plant DNA C-values database (release 7.1): an updated online repository of
668 plant genome size data for comparative studies. *New Phytol.* **226**, 301–305 (2020).

669 22. R. M. Waterhouse *et al.*, BUSCO applications from quality assessments to gene prediction and
670 phylogenomics. *Mol. Biol. Evol.* **35**, 543–548 (2018).

671 23. M. I. Love, W. Huber, S. Anders, Moderated estimation of fold change and dispersion for RNA-seq data
672 with DESeq2. *Genome Biol.* **15**, 550 (2014).

673 24. H. Wang, S. Zou, Y. Li, F. Lin, D. Tang, An ankyrin-repeat and WRKY-domain-containing immune receptor
674 confers stripe rust resistance in wheat. *Nat. Commun.* **11**, 1353 (2020).

675 25. S. G. Krattinger *et al.*, A putative ABC transporter confers durable resistance to multiple fungal
676 pathogens in wheat. *Science*. **323**, 1360–1363 (2009).

677 26. S. Chen *et al.*, Wheat gene Sr60 encodes a protein with two putative kinase domains that confers
678 resistance to stem rust. *New Phytol.* **225**, 948–959 (2020).

679 27. M. Dmochowska-Boguta *et al.*, TaWAK6 encoding wall-associated kinase is involved in wheat resistance
680 to leaf rust similar to adult plant resistance. *PLoS One*. **15**, e0227713 (2020).

681 28. M. Nyine *et al.*, Genomic Patterns of Introgression in Interspecific Populations Created by Crossing
682 Wheat with Its Wild Relative. *G3 (Bethesda)*. **10**, 3651–3661 (2020).

683 29. L.-J. Gardiner *et al.*, Analysis of the recombination landscape of hexaploid bread wheat reveals genes

684 controlling recombination and gene conversion frequency. *Genome Biol.* **20**, 69 (2019).

685 30. H. Li *et al.*, Introgression of the Aegilops speltoides Su1-Ph1 Suppressor into Wheat. *Front. Plant Sci.* **8**,
686 2163 (2017).

687 31. S. Walkowiak *et al.*, Multiple wheat genomes reveal global variation in modern breeding. *Nature*. **588**,
688 277–283 (2020).

689 32. A. M. Przewieslik-Allen *et al.*, The role of gene flow and chromosomal instability in shaping the bread
690 wheat genome. *Nat. Plants*. **7**, 172–183 (2021).

691 33. E. Rey *et al.*, Transcriptome reprogramming due to the introduction of a barley telosome into bread
692 wheat affects more barley genes than wheat. *Plant Biotechnol. J.* **16**, 1767–1777 (2018).

693 34. Z. Dong *et al.*, Genome-wide impacts of alien chromatin introgression on wheat gene transcriptions. *Sci.*
694 *Rep.* **10**, 4801 (2020).

695 35. S. Zheng *et al.*, Characterization and diagnostic marker development for Yr28-rga1 conferring stripe rust
696 resistance in wheat. *Eur. J. Plant Pathol.* **156**, 623–634 (2020).

697 36. J. G. Ellis, E. S. Lagudah, W. Spielmeyer, P. N. Dodds, The past, present and future of breeding rust
698 resistant wheat. *Front. Plant Sci.* **5**, 641 (2014).

699 37. A. M. Bolger, M. Lohse, B. Usadel, Trimmomatic: a flexible trimmer for Illumina sequence data.
700 *Bioinformatics*. **30**, 2114–2120 (2014).

701 38. G. M. Daly *et al.*, Host subtraction, filtering and assembly validations for novel viral discovery using next
702 generation sequencing data. *PLoS One*. **10**, e0129059 (2015).

703 39. International Wheat Genome Sequencing Consortium (IWGSC) *et al.*, Shifting the limits in wheat
704 research and breeding using a fully annotated reference genome. *Science*. **361** (2018),
705 doi:10.1126/science.aar7191.

706 40. H. Li, Aligning sequence reads, clone sequences and assembly contigs with BWA-MEM. **00**, 1–3 (2013).

707 41. H. Li *et al.*, The Sequence Alignment/Map format and SAMtools. *Bioinformatics*. **25**, 2078–2079 (2009).

708 42. M. A. DePristo *et al.*, A framework for variation discovery and genotyping using next-generation DNA
709 sequencing data. *Nat. Genet.* **43**, 491–498 (2011).

710 43. H. Li, A statistical framework for SNP calling, mutation discovery, association mapping and population
711 genetical parameter estimation from sequencing data. *Bioinformatics*. **27**, 2987–2993 (2011).

712 44. A. R. Quinlan, I. M. Hall, BEDTools: a flexible suite of utilities for comparing genomic features.
713 *Bioinformatics*. **26**, 841–842 (2010).

714 45. B. S. Pedersen, A. R. Quinlan, hts-nim: scripting high-performance genomic analyses. *Bioinformatics*. **34**,
715 3387–3389 (2018).

716 46. J. T. Robinson *et al.*, Integrative genomics viewer. *Nat. Biotechnol.* **29**, 24–26 (2011).

717 47. D. Thomson, R. Henry, Single-step protocol for preparation of plant tissue for analysis by PCR.
718 *BioTechniques*. **19**, 394–7, 400 (1995).

719 48. S. Grewal *et al.*, Development of Wheat-Aegilops caudata Introgression Lines and Their Characterization
720 Using Genome-Specific KASP Markers. *Front. Plant Sci.* **11**, 606 (2020).

721 49. W. De Coster, S. D'Hert, D. T. Schultz, M. Cruts, C. Van Broeckhoven, NanoPack: visualizing and
722 processing long-read sequencing data. *Bioinformatics*. **34**, 2666–2669 (2018).

723 50. H. Li, Minimap2: pairwise alignment for nucleotide sequences. *Bioinformatics*. **34**, 3094–3100 (2018).

724 51. B. J. Walker *et al.*, Pilon: an integrated tool for comprehensive microbial variant detection and genome
725 assembly improvement. *PLoS One*. **9**, e112963 (2014).

726 52. M. J. Roach, S. A. Schmidt, A. R. Borneman, Purge Haplotigs: allelic contig reassignment for third-gen
727 diploid genome assemblies. *BMC Bioinformatics*. **19**, 460 (2018).

728 53. D. M. Emms, S. Kelly, OrthoFinder: phylogenetic orthology inference for comparative genomics.
729 *Genome Biol.* **20**, 238 (2019).

730 54. S. Ou *et al.*, Benchmarking transposable element annotation methods for creation of a streamlined,
731 comprehensive pipeline. *Genome Biol.* **20**, 275 (2019).

732 55. C. Camacho *et al.*, BLAST+: architecture and applications. *BMC Bioinformatics*. **10**, 421 (2009).

733 56. W. Li, A. Godzik, Cd-hit: a fast program for clustering and comparing large sets of protein or nucleotide
734 sequences. *Bioinformatics*. **22**, 1658–1659 (2006).

735 57. N. Chen, Using RepeatMasker to identify repetitive elements in genomic sequences. *Curr Protoc*
736 *Bioinformatics*. **Chapter 4**, Unit 4.10 (2004), doi:10.1002/0471250953.bi0410s05.

737 58. A. Dobin *et al.*, STAR: ultrafast universal RNA-seq aligner. *Bioinformatics*. **29**, 15–21 (2013).

738 59. M. G. Grabherr *et al.*, Full-length transcriptome assembly from RNA-Seq data without a reference
739 genome. *Nat. Biotechnol.* **29**, 644–652 (2011).

740 60. M. Pertea *et al.*, StringTie enables improved reconstruction of a transcriptome from RNA-seq reads.
741 *Nat. Biotechnol.* **33**, 290–295 (2015).

742 61. C. Trapnell *et al.*, Differential gene and transcript expression analysis of RNA-seq experiments with
743 TopHat and Cufflinks. *Nat. Protoc.* **7**, 562–578 (2012).

744 62. L. Song, S. Sabunciyan, L. Florea, CLASS2: accurate and efficient splice variant annotation from RNA-seq
745 reads. *Nucleic Acids Res.* **44**, e98 (2016).

746 63. B. J. Haas *et al.*, De novo transcript sequence reconstruction from RNA-seq using the Trinity platform for
747 reference generation and analysis. *Nat. Protoc.* **8**, 1494–1512 (2013).

748 64. D. Mapleson, L. Venturini, G. Kaithakottil, D. Swarbreck, Efficient and accurate detection of splice
749 junctions from RNA-seq with Portcullis. *Gigascience*. **7** (2018), doi:10.1093/gigascience/giy131.

750 65. UniProt Consortium, UniProt: a worldwide hub of protein knowledge. *Nucleic Acids Res.* **47**, D506–D515
751 (2019).

752 66. L. Venturini, S. Caim, G. G. Kaithakottil, D. L. Mapleson, D. Swarbreck, Leveraging multiple transcriptome
753 assembly methods for improved gene structure annotation. *Gigascience*. **7** (2018),
754 doi:10.1093/gigascience/giy093.

755 67. G. S. C. Slater, E. Birney, Automated generation of heuristics for biological sequence comparison. *BMC*
756 *Bioinformatics*. **6**, 31 (2005).

757 68. K. J. Hoff, M. Stanke, Predicting Genes in Single Genomes with AUGUSTUS. *Curr Protoc Bioinformatics*.
758 **65**, e57 (2019).

759 69. B. J. Haas *et al.*, Automated eukaryotic gene structure annotation using EVidenceModeler and the
760 Program to Assemble Spliced Alignments. *Genome Biol.* **9**, R7 (2008).

761 70. W. H. Majoros, M. Pertea, S. L. Salzberg, TigrScan and GlimmerHMM: two open source ab initio
762 eukaryotic gene-finders. *Bioinformatics*. **20**, 2878–2879 (2004).

763 71. I. Korf, Gene finding in novel genomes. *BMC Bioinformatics*. **5**, 59 (2004).

764 72. T. Wicker, D. E. Matthews, B. Keller, TREP: a database for Triticeae repetitive elements. *Trends Plant Sci.*
765 **7**, 561–562 (2002).

766 73. A. Bairoch, R. Apweiler, The SWISS-PROT protein sequence data bank and its supplement TrEMBL.
767 *Nucleic Acids Res.* **25**, 31–36 (1997).

768 74. J. Huerta-Cepas *et al.*, eggNOG 5.0: a hierarchical, functionally and phylogenetically annotated

769 orthology resource based on 5090 organisms and 2502 viruses. *Nucleic Acids Res.* **47**, D309–D314
770 (2019).

771 75. D. Kim, J. M. Paggi, C. Park, C. Bennett, S. L. Salzberg, Graph-based genome alignment and genotyping
772 with HISAT2 and HISAT-genotype. *Nat. Biotechnol.* **37**, 907–915 (2019).

773 76. R. H. Ramírez-González *et al.*, The transcriptional landscape of polyploid wheat. *Science*. **361** (2018),
774 doi:10.1126/science.aar6089.

775 77. A. Alexa, J. Rahnenfuhrer, Gene set enrichment analysis with topGO (2020).

776 78. R. D. Finn, J. Clements, S. R. Eddy, HMMER web server: interactive sequence similarity searching.
777 *Nucleic Acids Res.* **39**, W29-37 (2011).

778 79. B. Steuernagel *et al.*, The NLR-Annotator Tool Enables Annotation of the Intracellular Immune Receptor
779 Repertoire. *Plant Physiol.* **183**, 468–482 (2020).

780 Acknowledgements

781 We would like to acknowledge BBS/E/T/000PR9816 (NC1 - Supporting EI's ISPs and the UK Community with
782 Genomics and Single Cell Analysis) for data generation and BB/CCG1720/1 for the physical HPC infrastructure
783 and data centre delivered via the NBI Computing infrastructure for Science (CiS) group.

784 **Funding:**

785 BBSRC Core Capability Grant BB/CCG1720/1 (AH)

786 BBSRC funded Norwich Research Park Biosciences Doctoral Training Partnership grant BB/M011216/1 (BC)

787 BBSRC Designing Future Wheat grant BB/P016855/1 and its constituent work packages DFW WP4 Data Access
788 and Analysis

789 **Author contributions:**

790 Conceptualization: AH, JL, IPK, BC

791 Methodology: BC, RJ, RR-P

792 Formal analysis: BC

793 Investigation: JF, SG, CY, SE

794 Writing - Original Draft: BC

Writing - Review & Editing: BC, AH, RR-P, JK, JF

Visualization: BC

Supervision: AH

Funding acquisition: AH, JK, IPK

Competing interests:

Authors declare that they have no competing interests

Data and materials availability:

Sequencing data produced as part of this study, along with the *Am. muticum* assembly is available at: https://opendata.earlham.ac.uk/wheat/under_license/toronto/Hall_2021-10-08_wheatxmuticum. [This data will be uploaded to the European Nucleotide Archive (ENA) while the paper is under review]. *Am. muticum* illumina sequencing data available at: https://opendata.earlham.ac.uk/wheat/under_license/toronto/Grewal_et_al_2021-09-13_Amybylopyrum_muticum/. The Chinese Spring sequencing data used is available from ENA (study PRJNA393343; runs SRR5893651 and SRR5893652). The Paragon sequencing data used is available from ENA (study PRJEB35709; runs ERR3728451, ERR3760033, ERR3760405 and ERR3728448). Custom scripts used for introgression detection are available at: https://github.com/benedictcoombes/alien_detection.